



NRC Publications Archive Archives des publications du CNRC

Formation of Pt-Ru nanoparticles in ethylene glycol solution: an in situ X-ray absorption spectroscopy study

Sarma, Loka Subramanyam; Chen, Ching-Hsiang; Kumar, Sakkarapalayam Murugesan Senthil; Wang, Guo-Rung; Yen, Shih-Chieh; Liu, Din-Goa; Sheu, Hwo-Shuenn; Yu, Kuan-Li; Tang, Mau-Tsu; Lee, Jyh-Fu; Bock, Christina; Chen, Kuei-Hsien; Hwang, Bing-Joe

This publication could be one of several versions: author's original, accepted manuscript or the publisher's version. / La version de cette publication peut être l'une des suivantes : la version prépublication de l'auteur, la version acceptée du manuscrit ou la version de l'éditeur.

For the publisher's version, please access the DOI link below. / Pour consulter la version de l'éditeur, utilisez le lien DOI ci-dessous.

Publisher's version / Version de l'éditeur:

<https://doi.org/10.1021/la0637418>

Langmuir, 23, 10, 2007

NRC Publications Record / Notice d'Archives des publications de CNRC:

<https://nrc-publications.canada.ca/eng/view/object/?id=29b3d2a8-77f1-49d8-a160-3911e57a5737>

<https://publications-cnrc.canada.ca/fra/voir/objet/?id=29b3d2a8-77f1-49d8-a160-3911e57a5737>

Access and use of this website and the material on it are subject to the Terms and Conditions set forth at

<https://nrc-publications.canada.ca/eng/copyright>

READ THESE TERMS AND CONDITIONS CAREFULLY BEFORE USING THIS WEBSITE.

L'accès à ce site Web et l'utilisation de son contenu sont assujettis aux conditions présentées dans le site

<https://publications-cnrc.canada.ca/fra/droits>

LISEZ CES CONDITIONS ATTENTIVEMENT AVANT D'UTILISER CE SITE WEB.

Questions? Contact the NRC Publications Archive team at

PublicationsArchive-ArchivesPublications@nrc-cnrc.gc.ca. If you wish to email the authors directly, please see the first page of the publication for their contact information.

Vous avez des questions? Nous pouvons vous aider. Pour communiquer directement avec un auteur, consultez la première page de la revue dans laquelle son article a été publié afin de trouver ses coordonnées. Si vous n'arrivez pas à les repérer, communiquez avec nous à PublicationsArchive-ArchivesPublications@nrc-cnrc.gc.ca.



Formation of Pt–Ru Nanoparticles in Ethylene Glycol Solution: An in Situ X-ray Absorption Spectroscopy Study

Loka Subramanyam Sarma,[†] Ching-Hsiang Chen,^{†,‡}
Sakkarapalayam Murugesan Senthil Kumar,[†] Guo-Rung Wang,[†] Shih-Chieh Yen,[†]
Din-Goa Liu,[§] Hwo-Shuenn Sheu,[§] Kuan-Li Yu,[§] Mau-Tsu Tang,[§] Jyh-Fu Lee,[§]
Christina Bock,^{||} Kuei-Hsien Chen,[‡] and Bing-Joe Hwang^{*,†,§}

Nanoelectrochemistry Laboratory, Department of Chemical Engineering, National Taiwan University of Science and Technology, Taipei 106, National Synchrotron Radiation Research Center, Hsinchu 30076, and Institute of Atomic and Molecular Sciences, Academia Sinica, Taipei 106, Taiwan, Republic of China, and National Research Council of Canada, 1200 Montreal Road, Ottawa, Ontario, Canada K1A 0R6

Received December 27, 2006. In Final Form: February 22, 2007

The chemical state and formation mechanism of Pt–Ru nanoparticles (NPs) synthesized by using ethylene glycol (EG) as a reducing agent and their stability have been examined by in situ X-ray absorption spectroscopy (XAS) at the Pt L_{III} and Ru K edges. It appears that the reduction of Pt(IV) and Ru(III) precursor salts by EG is not a straightforward reaction but involves different intermediate steps. The pH control of the reaction mixture containing Pt(IV) and Ru(III) precursor salts in EG to 11 led to the reduction of Pt(IV) to Pt(II) corresponding to [PtCl₄]²⁻ whereas Ru^{III}Cl₃ is changed to the [Ru(OH)₆]³⁻ species. Refluxing the mixture containing [PtCl₄]²⁻ and [Ru(OH)₆]³⁻ species at 160 °C for 0.5 h produces Pt–Ru NPs as indicated by the presence of Pt and Ru in the first coordination shell of the respective metals. No change in XAS structural parameters is found when the reaction time is further increased, indicating that the Pt–Ru NPs formed are extremely stable and less prone to aggregation. XAS structural parameters suggest a Pt-rich core and a Ru-rich shell structure for the final Pt–Ru NPs. Due to the inherent advantages of the EG reduction method, the atomic distribution and alloying extent of Pt and Ru in the Pt–Ru NPs synthesized by the EG method are higher than those of the Pt–Ru/C NPs synthesized by a modified Watanabe method.

Introduction

Highly dispersed and size-selected carbon-supported Pt–Ru catalyst nanoparticles (NPs) have received extensive attention due to their application as catalysts for the electrooxidation of methanol in direct methanol fuel cells (DMFCs).¹ The intrinsic properties of PtRu/C NPs are mainly determined by their size, composition, distribution of Pt and Ru sites at the atomic level, homogeneity, and surface population of Pt and Ru.² In principle, one could control any one of these parameters to fine-tune the properties of these nanoparticles, and it is beneficial to tune their catalytic performance. Many synthesis methods appearing in the literature consider the particle homogeneity as the main criterion in preparing PtRu/C NPs, while some studies focus on the Pt and Ru distribution.³ In a recent work of Bock et al., PtRu/C NPs were prepared within the range of 0.7–4 nm by controlling the pH of the reaction medium in ethylene glycol solutions.^{1a} Depending on the pH of the medium, ethylene glycol will be oxidized to glycolic acid or glycolate anion. The glycolate anion formed acts as a stabilizer for the PtRu colloids, and its concentration, and hence the resulting PtRu particle size, is controlled via the synthesis solution pH. Even though considerable work has been done in formulating the strategies to control the

size and size distribution of metal nanoparticles by the polyol process, studies focused on controlling the distribution of Pt and Ru sites of PtRu/C NPs and their stability during the synthesis process are limited. Recently, on the basis of XAS methodology, we have shown that the alloying extent or atomic distribution in nanoparticles is an important factor of concern that has a strong influence on their catalytic activities.⁴ Hence, we believe that the polyol process will be more effective for the control of the Pt and Ru atomic distribution and stability of Pt–Ru NPs. To achieve this atomic level information, a detailed understanding of the metal nanoparticle formation mechanism is essential. Also success in either particle design or scaleup requires a detailed knowledge of the particle formation mechanism and will greatly benefit the development of needed structure-controllable synthetic pathways for metal nanoparticles.

X-ray absorption spectroscopy (XAS) is a powerful complementary tool for investigating structural evolution, and in many cases the structural properties of metal particles can be probed in situ during the different steps of preparation. Other techniques such as X-ray diffraction (XRD) and transmission electron microscopy (TEM)⁵ are difficult to employ during in situ conditions because the nanoparticle structure would change during the preparation or transportation of the sample or by the lack of long-range ordering.⁶ It has been shown in the literature that study in the X-ray absorption near-edge spectroscopy (XANES) region (conventionally from below the edge up to ~30–50 eV)

* To whom correspondence should be addressed. Fax: +886-2-27376644. E-mail: bjh@mail.ntust.edu.tw.

[†] National Taiwan University of Science and Technology.

[‡] Academia Sinica.

[§] National Synchrotron Radiation Research Center.

^{||} National Research Council of Canada.

(1) (a) Bock, C.; Paquet, C.; Couillard, M.; Botton, G. A.; MacDougall, B. R. *J. Am. Chem. Soc.* **2004**, *126*, 8028. (b) Hogarth, M. P.; Hards, G. A. *Platinum Met. Rev.* **1996**, *40*, 150.

(2) Frenkel, A. I.; Wills, C. W.; Nuzzo, R. G. *J. Phys. Chem. B* **2001**, *105*, 12689.

(3) Hwang, B. J.; Chen, C. H.; Sarma, L. S.; Chen, J. M.; Wang, G. R.; Tang, M. T.; Liu, D. G.; Lee, J. F. *J. Phys. Chem. B* **2006**, *110*, 6475.

(4) Hwang, B. J.; Sarma, L. S.; Chen, J. M.; Chen, C. H.; Shih, S. C.; Wang, G. R.; Liu, D. G.; Lee, J. F.; Tang, M. T. *J. Am. Chem. Soc.* **2005**, *127*, 11140.

(5) (a) Zhang, Z. C.; Lei, G. D.; Sachtler, W. M. H. In *Series on Synchrotron Radiation Techniques and Applications*; Iwasawa, Y., Ed.; World Scientific: Singapore, 1996; Vol. 2, p 137. (b) Ashcroft, A. T.; Cheetham, A. K.; Harris, P. J. F.; Jones, R. H.; Natarajan, S.; Sankar, G.; Stedman, N. J.; Thomas, J. M. *Catal. Lett.* **1994**, *24*, 47.

(6) Cao, D.; Bergens, H. J. *Power Sources* **2004**, *134*, 170.

provides information about the oxidation state, fractional d-electron density, and electronic environment of the absorbing atom. Spectra obtained from the region extending from the XANES region to as high as 2 keV above the edge are known as the extended X-ray absorption fine structure (EXAFS) spectra and are primarily due to the scattering of the photoelectron off near-neighbor atoms. The amplitude of the EXAFS function $\chi(k)$, where k is the wave vector, is proportional to the number of nearest neighbors, and the change of phase with the wavelength of the photoelectron depends on the distance between the emitter and the backscattering atom.⁷ The backscattering strength also depends on the type or atomic number of atoms involved in the backscattering process. Thus, an analysis of EXAFS data yields structural details about the absorbing atom and its local environment. In recent years XAS studies have been well explored on bimetallic nanoparticles,⁸ and we utilized XAS to study the mechanism of mono- and bimetallic nanoparticle formation.^{3,9} The electronic and structural properties of nanometer-scale metallic clusters have been widely studied by utilizing the L edge XANES. Recently, Bazin et al. have used a combined full multiple scattering (MS) and principal component analysis (PCA) approach for the K edge XANES analysis of nanometer-scale transition metals. The combined MS and PCA approach offers a better understanding of the physicochemical processes specific to nanometer-scale entities.¹⁰ In situ XAS allows investigation of the properties of Pt–Ru catalyst particles under working conditions similar to those of an actual fuel cell. Even though XAS has been applied to the study of fuel cell electrocatalysts, its application during the formation of Pt–Ru nanoparticles has remained relatively less explored. Wide-angle X-ray scattering (WAXS) is another suitable technique to gain structural insight into Pt–Ru nanoparticles.¹¹

In this study, we take up the investigation of the formation mechanism, the resulting Pt and Ru atomic distributions in the cluster, and the structure of Pt–Ru NPs synthesized by the polyol process by following the in situ X-ray absorption spectra recorded at the Pt L_{III} edge (11564 eV) and Ru K edge (22117 eV). Our results show that the distribution of Pt and Ru in the PtRu/C NPs synthesized by the polyol process is increased compared to the Pt and Ru distribution in the PtRu/C NPs synthesized by the modified Watanabe method.³

Experimental Section

Synthesis of Pt–Ru Nanoparticles. Reagent grade reducing agent, i.e., ethylene glycol (EG), was obtained from Acros, and Pt and Ru precursor salts, i.e., H₂PtCl₆·xH₂O and RuCl₃, were purchased

from Alfa Aesar. They were used as-received without further purification. First 10 mL of 0.25 M H₂PtCl₆ in EG and 10 mL of 0.25 M RuCl₃ in EG were mixed together for 30 min at room temperature. Later, the pH of the reaction mixture was adjusted to 11 by adding 1 M NaOH dropwise. Subsequently, the reaction solutions were heated under reflux at 160 °C for four time periods of 0.5, 1, 2, and 4 h. After reflux at each time period the reaction mixture was cooled to room temperature and subjected to the XAS measurements.

High-Resolution (HR) TEM Measurements. The high-resolution TEM image of the final Pt–Ru NPs was obtained by using a Philips/FEI Tecnai 20G2 S-Twin TEM apparatus. For TEM analyses, the sample was prepared by ultrasonically suspending Pt–Ru NPs in ethanol solution, the sample was applied to a carbon-coated copper grid, and the solvent was evaporated in a vacuum drybox at room temperature.

In Situ XAS Measurements. The X-ray absorption spectra were recorded on Taiwan beamline BL12B2 at Spring-8, Hyogo, Japan, and on beamline BL01C1 at the National Synchrotron Radiation Research Center, Taiwan. The electron storage ring of Spring-8 was operated at 8 GeV. A double Si(111) crystal monochromator was employed for energy selection with a resolution $\Delta E/E$ better than 1×10^{-4} at both the Pt L_{III} edge (11564 eV) and the Ru K edge (22117 eV). The reaction mixture at different stages of Pt–Ru nanoparticle formation, i.e., including the mixing of the Pt and Ru precursors in EG solution and adjustment of the pH of the reaction mixture and after cooling of the refluxed reaction mixture at 160 °C for four time periods of 0.5, 1, 2, and 4 h, was taken in a homemade cell made of PTFE for XAS study. Two holes were made, one on top of the cell and the other on one side. After placement of the liquid samples, the top hole was closed with a Teflon rod to avoid exposure of the sample to the outer atmosphere. A hollow Teflon rod with a Kapton film cap at one end was inserted into the other hole in the XAS cell. The position of the Teflon rod was adjusted to reach the optimum absorption thickness ($\Delta\mu x \approx 1.0$, $\Delta\mu$ being the absorption edge and x the thickness of the liquid layer) so that the proper edge jump step could be achieved during the measurements. All of the spectra were recorded at room temperature in transmission mode. Higher harmonics were eliminated by detuning the double crystal Si(111) monochromator. Three gas-filled ionization chambers were used in series to measure the intensities of the incident beam (I_0), the beam transmitted by the sample (I_s), and the beam subsequently transmitted by the reference foil (I_r). The third ion chamber was used in conjunction with the reference sample, which was a Pt foil for Pt L_{III} edge measurements and Ru powder for Ru K edge measurements. The control of parameters for EXAFS measurements, data collection modes, and calculation of errors were all done as per the guidelines set by the International XAFS Society Standards and Criteria Committee.¹²

XAS Data Analysis. The EXAFS data reduction was conducted by utilizing the standard procedures. The EXAFS function, χ , was obtained by subtracting the postedge background from the overall absorption and then normalized with respect to the edge jump step. The normalized $\chi(E)$ was transformed from energy space to k space, where k is the photoelectron wave vector. The $\chi(k)$ data were multiplied by k^2 to compensate the damping of EXAFS oscillations in the high k region. Subsequently, k^2 -weighted $\chi(k)$ data in k space ranging from 3.6 to 12.6 Å⁻¹ for the Pt L_{III} edge and from 3.6 to 11.6 Å⁻¹ for the Ru K edge were Fourier transformed to r space to separate the EXAFS contributions from the different coordination shells. A nonlinear least-squares algorithm was applied to the curve fitting of an EXAFS in r space between 0.7 and 3.3 Å for both Pt and Ru depending on the bond to be fitted. For the Pt–Ru reference file a suitable experimental reference compound was not available for calibration purposes. Hence, the effective scattering amplitude [$f(k)$] and phase shift [$\delta(k)$] for Pt–Ru were generated by using the

(7) (a) Teo, B. K. *EXAFS. Basic Principles and Data Analysis*; Springer: Berlin, Germany, 1986. (b) Bianconi, A. In *X-ray Absorption: Principles, Applications, Techniques of EXAFS, SEXAFS, and XANES*; Prins, R., Koningsberger, D. E., Eds.; Wiley-Interscience: New York, 1988.

(8) (a) Park, J.-I.; Kim, M. G.; Jun, Y.; Lee, J. S.; Lee, W.; Cheon, J. *J. Am. Chem. Soc.* **2004**, *126*, 9072. (b) Nashner, M. S.; Frenkel, A. I.; Adler, D. L.; Shapley, J. R.; Nuzzo, R. G. *J. Am. Chem. Soc.* **1997**, *119*, 7760. (c) O'Grady, W. E.; Hagans, P. L.; Pandya, K. I.; Maricle, D. L. *Langmuir* **2001**, *17*, 3047. (d) Hills, C. W.; Nashner, M. S.; Frenkel, A. I.; Shapley, J. R.; Nuzzo, R. G. *Langmuir* **1999**, *15*, 690. (e) Nashner, M. S.; Frenkel, A. I.; Somerville, D.; Hills, C. W.; Shapley, J. R.; Nuzzo, R. G. *J. Am. Chem. Soc.* **1998**, *120*, 8093. (f) Toshima, N.; Harada, M.; Yonezawa, T.; Kushihashi, K.; Asakura, K. *J. Phys. Chem.* **1991**, *95*, 7448. (g) Bian, C.-R.; Suzuki, S.; Asakura, K.; Ping, L.; Toshima, N. *J. Phys. Chem. B* **2002**, *106*, 8587.

(9) (a) Tsai, Y. W.; Tseng, Y. L.; Sarma, L. S.; Liu, D. G.; Lee, J.-F.; Hwang, B. J. *J. Phys. Chem. B* **2004**, *108*, 8148. (b) Hwang, B.-J.; Tsai, Y. W.; Sarma, L. S.; Liu, D. G.; Lee, J. F. *J. Phys. Chem. B* **2004**, *108*, 20427. (c) Chen, C.-H.; Hwang, B.-J.; Wang, G.-R.; Sarma, L. S.; Tang, M.-T.; Liu, D.-G.; Lee, J.-F. *J. Phys. Chem. B* **2005**, *109*, 21566. (d) Chen, C.-H.; Sarma, L. S.; Wang, G. R.; Chen, J. M.; Shih, S. C.; Tang, M. T.; Liu, D. G.; Lee, J. F.; Chen, J. M.; Hwang, B.-J. *J. Phys. Chem. B* **2006**, *110*, 10287.

(10) Bazin, D.; Rehr, J. J. *J. Phys. Chem. B* **2003**, *107*, 12398.

(11) Dassenoy, F.; Casanove, M. J.; Lecante, P.; Pan, C.; Philippot, K.; Amiens, C.; Chaudret, B. *Phys. Rev. B* **2001**, *63*, 235407.

(12) (a) See, for example, the guidelines for data collection modes for EXAFS measurements and user-controlled parameters: http://ixs.iit.edu/subcommittee_reports/sc/sc00report.pdf. (b) See, for example, the guidelines for error reporting: http://ixs.iit.edu/subcommittee_reports/sc/err-rep.pdf.

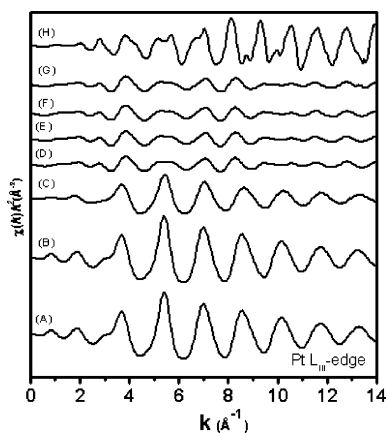


Figure 1. Raw $k^2\chi(k)$ (\AA^{-2}) EXAFS data of the Pt L_{III} edge measured for various reaction steps during the formation of Pt–Ru nanoparticles in EG solutions and the reference Pt foil: (A) 0.25 M H_2PtCl_6 in EG, (B) 0.25 M H_2PtCl_6 in EG + 0.25 M RuCl_3 in EG, (C) pH control to 11, (D) reflux at 160 °C, 0.5 h, (E) reflux at 160 °C, 1 h, (F) reflux at 160 °C, 2 h, (G) reflux at 160 °C, 4 h, (H) Pt foil.

FEFF7 code by keeping the Pt atoms at (0, 1/2, 1/2), (1/2, 0, 1/2), and (1/2, 1/2, 0) and Ru in the (0, 0, 0) position in a cubic unit cell of the close packing model. The lattice parameter $a = 3.83 \text{ \AA}$ is used in the FEFF7 calculation. The reference phase and amplitude for the Pt–Pt and Pt–Cl absorber–scatterer pairs were obtained from a Pt foil and H_2PtCl_6 , respectively. For Ru–Ru and Ru–O absorber–scatterer pairs the phase and amplitude were obtained from reference Ru powder and RuO_2 , respectively. All the computer programs were implemented in the UWXAFS 3.0 package,¹³ with the backscattering amplitude and the phase shift for the specific atom pairs being theoretically calculated by using the FEFF7 code.¹⁴ From these analyses, structural parameters such as the coordination numbers (N), bond distance (R), and Debye–Waller factor ($\Delta\sigma^2$) and the inner potential shift (ΔE_0) have been calculated. The amplitude reduction factor (S_0^2) values, which account for energy loss due to multiple excitations, for Pt and Ru were obtained by analyzing the Pt foil and Ru powder reference samples, respectively, and by fixing the coordination number in the FEFFIT input file. The S_0^2 values were found to be 0.95 and 0.88 for Pt and Ru, respectively.

Results and Discussion

Figure 1 displays the raw background-subtracted k^2 -weighted Pt L_{III} edge EXAFS data ($\Delta k = 3.6\text{--}12.6 \text{ \AA}^{-1}$) collected from all the reaction steps during the formation of Pt–Ru NPs and the Pt reference foil. A high signal-to-noise ratio of the data allows EXAFS oscillations to be clearly observed up to 14 \AA^{-1} and shows good data quality.

The XANES spectra for all the reaction steps during the formation of Pt–Ru NPs and for reference Pt foil are depicted in Figure 2. The XANES profile of the Pt precursor, i.e., H_2PtCl_6 in EG, exhibits a sharp peak positioned at 11567 eV, about 1.5 eV above the Pt metal's edge corresponding to the +4 oxidation state of Pt.^{9a} This sharp peak is generally called a white line, and its intensity is sensitive to the degree of electron occupancy in the valence orbitals of the absorber.¹⁵ The variation in the white line intensity will give information about the oxidation state of Pt in the compounds. Generally, the lower the white line intensity, the higher the electron density and lower the oxidation state of Pt. As can be seen from Figure 2, there is no change in the white line intensity of H_2PtCl_6 in EG after mixing with RuCl_3 in EG

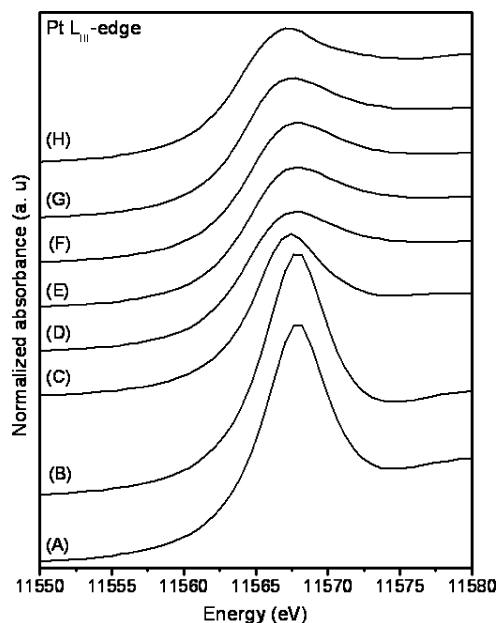


Figure 2. In situ Pt L_{III} edge XANES spectra for various reaction steps during the formation of Pt–Ru nanoparticles in EG solutions and the Pt reference foil: (A) 0.25 M H_2PtCl_6 in EG, (B) 0.25 M H_2PtCl_6 in EG + 0.25 M RuCl_3 in EG, (C) pH control to 11, (D) reflux at 160 °C, 0.5 h, (E) reflux at 160 °C, 1 h, (F) reflux at 160 °C, 2 h, (G) reflux at 160 °C, 4 h, (H) Pt foil.

solution, indicating that the platinum is still in the +4 oxidation state. However, when the pH of the reaction mixture containing Pt^{4+} and Ru^{3+} ions is adjusted to 11 by the addition of 1 M NaOH, a sharp decrease in the white line intensity is observed, indicating that Pt^{4+} ions are reduced to Pt^{2+} ions. However, chemical speciation of the compound formed in this step is difficult to explain with the XANES results alone, and we will discuss it in detail during the discussion of the EXAFS results. The progressive reduction (or initiation of reduction) prior to reflux of the reaction mixture at higher temperature is a crucial observation, as it influences the nucleation and growth of particles, which in turn have an impact on the size, distribution, and alloying extent of the final nanoparticles.

It is known that ethylene glycol will act both as a solvent and as a reducing agent in the so-called polyol process available for the synthesis of metal nanoparticles. However, the reduction ability of EG is dependent on the pH of the reaction medium and influences the size of the final metal particles.^{1a} Unfortunately, no attempt was made at the chemical speciation of Pt and Ru during the pH control step of the EG reduction method in previous studies, and the present XAS studies are quite helpful. After the reaction mixture is refluxed for 0.5 h, the intensity of the white line is significantly decreased, and it is now close to the white line intensity of the Pt foil. Longer reflux times do not change the intensity of the white line. Thus, XANES results clearly demonstrate that Pt^{2+} ions are reduced to Pt^0 within less than 0.5 h of reflux time, and Pt^0 is stable at further reaction times. A slightly higher white line intensity observed for the final Pt–Ru particles compared to the Pt foil is an indication that the formed Pt–Ru particles are in the nanometer regime.

Figure 3 represents typical raw k^2 -weighted Ru K edge EXAFS data ($\Delta k = 3.6\text{--}11.6 \text{ \AA}^{-1}$) collected from all the reaction steps during the formation of Pt–Ru NPs and the Ru powder reference. One can notice a very good signal-to-noise ratio with good data quality.

Figure 4 shows the XANES patterns recorded at various reaction steps during the formation of Pt–Ru nanoparticles and

(13) Stern, E. A.; Neville, M.; Ravel, B.; Yacoby, Y.; Haskel, D. *Physica B* **1995**, 208–209, 117.

(14) Zabinsky, S. I.; Rehr, J. J.; Anukodinov, A. L.; Albers, R. C.; Eller, M. J. *Phys. Rev. B* **1995**, 52, 2995.

(15) Horsely, J. A. *J. Chem. Phys.* **1982**, 76, 1451.

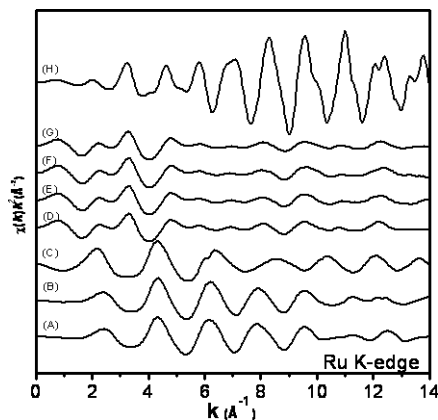


Figure 3. Raw $k^2\chi(k)$ (\AA^{-2}) EXAFS data of the Ru K edge measured for various reaction steps during the formation of Pt–Ru nanoparticles in EG solutions and the Ru powder reference: (A) 0.25 M H_2PtCl_6 in EG, (B) 0.25 M H_2PtCl_6 in EG + 0.25 M RuCl_3 in EG, (C) pH control to 11, (D) reflux at 160 °C, 0.5 h, (E) reflux at 160 °C, 1 h, (F) reflux at 160 °C, 2 h, (G) reflux at 160 °C, 4 h, (H) Ru powder reference.

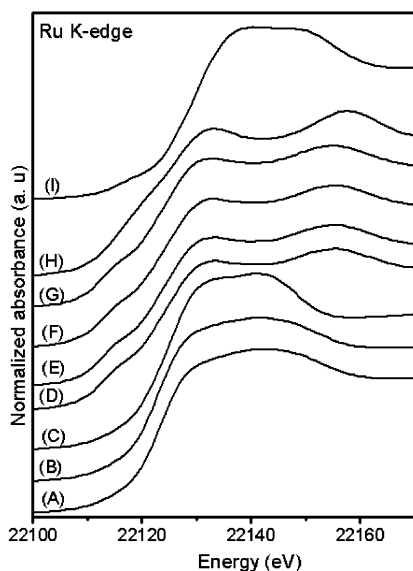


Figure 4. In situ Ru K edge XANES spectra for various reaction steps during the formation of Pt–Ru nanoparticles in EG solutions and the reference materials: (A) 0.25 M H_2PtCl_6 in EG, (B) 0.25 M H_2PtCl_6 in EG + 0.25 M RuCl_3 in EG, (C) pH control to 11, (D) reflux at 160 °C, 0.5 h, (E) reflux at 160 °C, 1 h, (F) reflux at 160 °C, 2 h, (G) reflux at 160 °C, 4 h, (H) Ru powder reference, (I) RuO_2 reference.

reference Ru powder. The XANES patterns of the Ru precursor, i.e., RuCl_3 dissolved in EG, exhibit a sharp peak with an edge positioned between Ru powder and RuO_2 reference compounds. No change in the XANES profile is observed when RuCl_3 in EG solution is mixed with H_2PtCl_6 in EG solution. Upon adjustment of the pH of the RuCl_3 and H_2PtCl_6 mixture in EG to 11, the peak intensity is increased sharply without the edge position being changed, indicating that the ligand environment around the Ru^{3+} ions is changed. We believe that the pH treatment led to the OH environment around Ru^{3+} , and the species formed at this stage will be confirmed with EXAFS results. Refluxing the reaction mixture at 160 °C for 0.5 h led to a shift in the edge energy to a lower value by about 3 eV, indicating that Ru^{3+} ions are reduced to Ru^0 . The edge energy position is closely matched with that of the Ru reference at this stage, indicating that most of the Ru^{3+} ions are reduced. Similar to the Pt L_{III} edge XANES, Ru K edge

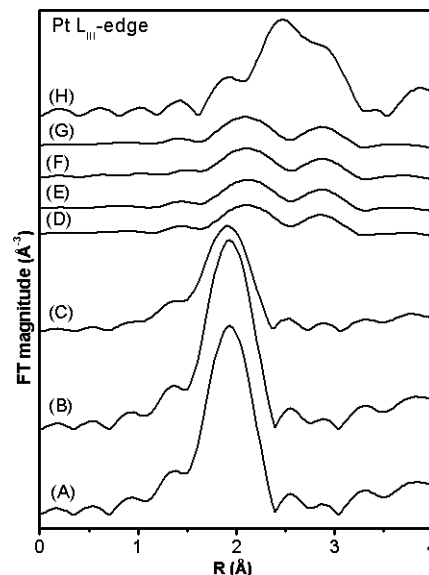


Figure 5. Pt L_{III} edge FT-EXAFS spectra for various reaction steps during the formation of Pt–Ru nanoparticles in EG solutions and the reference Pt foil: (A) 0.25 M H_2PtCl_6 in EG, (B) 0.25 M H_2PtCl_6 in EG + 0.25 M RuCl_3 in EG, (C) pH control to 11, (D) reflux at 160 °C, 0.5 h, (E) reflux at 160 °C, 1 h, (F) reflux at 160 °C, 2 h, (G) reflux at 160 °C, 4 h, (H) Pt foil.

XANES also shows that there is no change in the peak profile after refluxing of the reaction mixture, further supporting the stability of Pt–Ru NPs.

The modules of the Fourier transform (FT) of the various reaction steps during the formation of Pt–Ru NPs are shown in Figure 5. XAS fitting parameters are listed in Table 1. The transform for the starting compound, i.e., H_2PtCl_6 in EG, exhibits a strong peak at 2.0 Å characteristic of the presence of a Pt–Cl bond. The position and nature of the peak and the number of chlorine atoms are found to be comparable with the XAS parameters given in the literature.¹⁶ Mixing H_2PtCl_6 in EG with RuCl_3 in EG solution does not change the magnitude of the Pt–Cl peak, suggesting that there is no change in the local environment of the Pt^{4+} ions. The important result is that a sharp decrease in the Pt–Cl peak magnitude is observed when the pH of the reaction mixture, i.e., H_2PtCl_6 in EG with RuCl_3 in EG solution, is controlled to 11. The contribution of the Pt–Cl peak with an average coordination number of 3.8 at a distance of 2.311 Å suggests that Pt^{4+} ions of H_2PtCl_6 are reduced to Pt^{2+} ions during the pH control step.^{9a} Refluxing the reaction mixture after pH control at 160 °C for 0.5 h leads to the formation of Pt–Ru particles as suggested by the presence of contributions from Pt–Ru correlations in FT-EXAFS spectra. The stability of the formed Pt–Ru NPs is further evidenced from no change in the FT-EXAFS spectral features after the reaction time is increased, and these results are consistent with XANES observations.

The FT-EXAFS spectra collected at the Ru K edge for different reaction steps and the Ru powder reference are shown in Figure 6. The different coordination numbers and interatomic distances of the first shell, obtained by fitting the data, are given in Table 2.

The RuCl_3 in EG solution FT-EXAFS spectrum shows a maximum between 1.4 and 2.3 Å corresponding to the nearest chlorine neighbors of Ru. $N_{\text{Ru-Cl}}$ is found to be 6.0 with a Ru–Cl bond length of 2.32 Å. The FT feature of RuCl_3 is not altered

(16) Ayala, R.; Sánchez Marcos, E.; Díaz-Moreno, S.; Armando Solé, V.; Muñoz-Páez, A. *J. Phys. Chem. B* 2001, 105, 7598.

Table 1. Best Fit Parameters Obtained from the Analysis of the Pt L_{III} Edge EXAFS Spectra of Various Reaction Steps during the Formation of Pt–Ru NPs in EG Solutions^a

reaction state	shell	<i>N</i>	<i>R</i> (Å)	$\sigma^2 (\times 10^{-3})$ (Å ²)	ΔE_0 (eV)	<i>R</i> factor
H ₂ PtCl ₆ in EG	Pt–Cl	5.6 (±0.2)	2.327 (±0.004)	2.8 (±0.2)	8.6 (±0.3)	0.0111
H ₂ PtCl ₆ + RuCl ₃ in EG	Pt–Cl	5.6 (±0.2)	2.326 (±0.003)	2.6 (±0.2)	8.5 (±0.3)	0.0107
pH control to 11	Pt–Cl	3.8 (±0.3)	2.311 (±0.003)	4.8 (±0.1)	7.5 (±0.2)	0.0155
reflux at 160 °C, 0.5 h	Pt–Ru	2.7 (±0.2)	2.745 (±0.004)	12.0 (±0.6)	0.8 (±0.5)	
	Pt–Pt	6.5 (±0.4)	2.772 (±0.004)	12.0 (±0.4)	7.3 (±0.9)	0.0350
reflux at 160 °C, 1 h	Pt–Ru	2.7 (±0.2)	2.743 (±0.003)	11.0 (±0.5)	0.8 (±0.5)	
	Pt–Pt	6.5 (±0.4)	2.770 (±0.004)	11.0 (±0.4)	7.1 (±1.0)	0.0370
reflux at 160 °C, 2 h	Pt–Ru	2.7 (±0.2)	2.741 (±0.003)	11.0 (±0.5)	−0.2 (±0.6)	
	Pt–Pt	6.5 (±0.5)	2.769 (±0.005)	11.0 (±0.4)	7.1 (±1.1)	0.0420
reflux at 160 °C, 4 h	Pt–Ru	2.7 (±0.2)	2.745 (±0.003)	11.0 (±0.4)	2.7 (±0.4)	
	Pt–Pt	6.5 (±0.3)	2.771 (±0.004)	12.0 (±0.3)	7.3 (±0.7)	0.0340

^a *N* = coordination number, *R* = coordination distance, σ^2 = Debye–Waller factor, and ΔE_0 = inner potential correction.

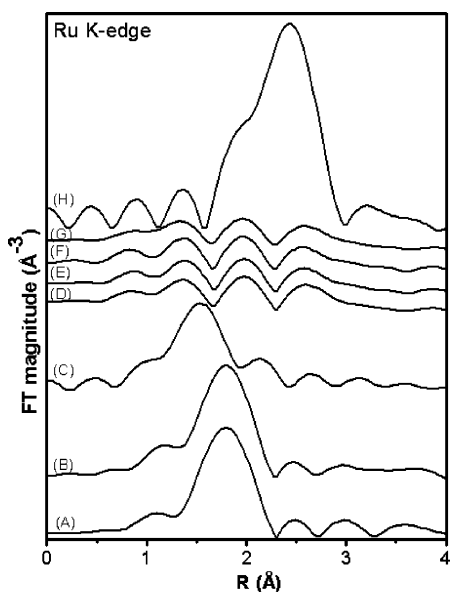


Figure 6. Ru K edge FT-EXAFS spectra for various reaction steps during the formation of Pt–Ru nanoparticles in EG solutions and the Ru powder reference: (A) 0.25 M H₂PtCl₆ in EG, (B) 0.25 M H₂PtCl₆ in EG + 0.25 M RuCl₃ in EG, (C) pH control to 11, (D) reflux at 160 °C, 0.5 h, (E) reflux at 160 °C, 1 h, (F) reflux at 160 °C, 2 h, (G) reflux at 160 °C, 4 h, (H) Ru powder reference.

after the addition of H₂PtCl₆ in EG solution to RuCl₃ in EG solution, indicating no change in the Ru–Cl contribution. Upon adjustment of the pH of the reaction mixture, i.e., a mixture of H₂PtCl₆ and RuCl₃ in EG solution, to 11, most of the Cl[−] coordination around Ru is rapidly transformed into OH[−] environments with a Ru–O distance of 2.052 Å. After the reaction mixture was refluxed at 160 °C for 0.5 h, an FT peak centered between 1.5 and 3 Å appeared, resulting from Ru–Pt and Ru–Ru bonding interactions, indicating the formation of Pt–Ru NPs. Similar to that of the Pt L_{III} edge, the Ru K edge FT-EXAFS too shows no change in FT magnitude after the reflux time is increased to 1, 2, and 4 h. The XAS results of the present study thus underscored that the Pt–Ru NPs formed by the polyol process possess good stability.

Formation Mechanism of Pt–Ru Nanoparticles. On the basis of the XAS results, we have attempted to discuss the formation mechanism of bimetallic Pt–Ru NPs. Comparing the FT-EXAFS spectra and fitting results of both the Pt L_{III} edge and the Ru K edge, a model is proposed for the mechanism of Pt–Ru NP formation and is shown in Scheme 1. From Pt L_{III} edge XAS, for the beginning compound H₂PtCl₆ in EG solution, we found *N*_{Pt–Cl} = 5.6, and it shows that the Pt⁴⁺ ion is surrounded by

nearly six chloride ions. The number of chlorine atoms found (slightly fewer than six) agrees with the constants given in the literature for the different acid and complex couples.¹⁷ Upon mixing of H₂PtCl₆ in EG with RuCl₃ in EG solution, *N*_{Pt–Cl} does not vary as realized from Pt L_{III} edge XAS, and *N*_{Ru–Cl} is found to be 6.0 as evidenced from the Ru K edge XAS. After control of the pH of the reaction mixture to 11, Pt L_{III} edge XAS shows that the coordination number (*N*_{Pt–Cl}) and the Pt–Cl interatomic distance (*R*_{Pt–Cl}) are found to be 3.8 and 2.311 Å, respectively, and are consistent with the constants related to anionic PtCl₄^{2−} ions.¹⁸

At the same reaction step, Ru K edge XAS reveal the presence of both OH[−] (*N*_{Ru–O} = 4.9) and Cl[−] (*N*_{Ru–Cl} = 0.5) environments around Ru. In fact, the real coordination number of OH[−] around Ru is underestimated since Cl[−] coordination is also used in the model. Hence, OH[−] coordination around Ru is higher, and these results indicate that the species produced at this stage are in the form of [Ru(OH)₆]^{3−}. Later refluxing the mixture containing PtCl₄^{2−} and [Ru(OH)₆]^{3−} ions at 160 °C for 0.5 h produces Pt and Ru coordination around Pt of 6.5 and 2.7, respectively and, similarly, Ru and Pt coordination around Ru of 2.8 and 2.7, respectively. All the coordination numbers and interatomic distances are not changed after the reflux time is increased, i.e., to 1, 2, and 4 h, indicating good stability of Pt–Ru NPs formed in EG solutions.

The ethylene glycol oxidation pathway during the formation of metal nanoparticles has been explained by analyzing the volatile compounds which result from the EG oxidation.¹⁹ Some researchers have mentioned that, among various compounds, diacetyl appears to be the main product, while some others reported that glycolic acid is the main oxidation product of ethylene glycol. Recently, Bock et al. carried out HPLC analysis to establish the dominating EG oxidation pathway by using the synthesis solutions after PtRu colloids were adsorbed on carbon.^{1a} They propose that initially ethylene glycol interacts with Pt and Ru ion sites and is oxidized to unstable aldehydes first, and these aldehydes are further oxidized to acids. They found both oxalic (COOH–COOH) and glycolic (CH₂OH–COOH) acid molecules in the chromatograms. However, on the basis of the concentrations of products and their electronic concentrations available for the reduction of Pt⁴⁺ and Ru³⁺, they concluded that 60% of the

(17) Shelimov, B.; Lambert, J. F.; Che, M.; Didillon, B. *J. Am. Chem. Soc.* **1999**, *121*, 545.

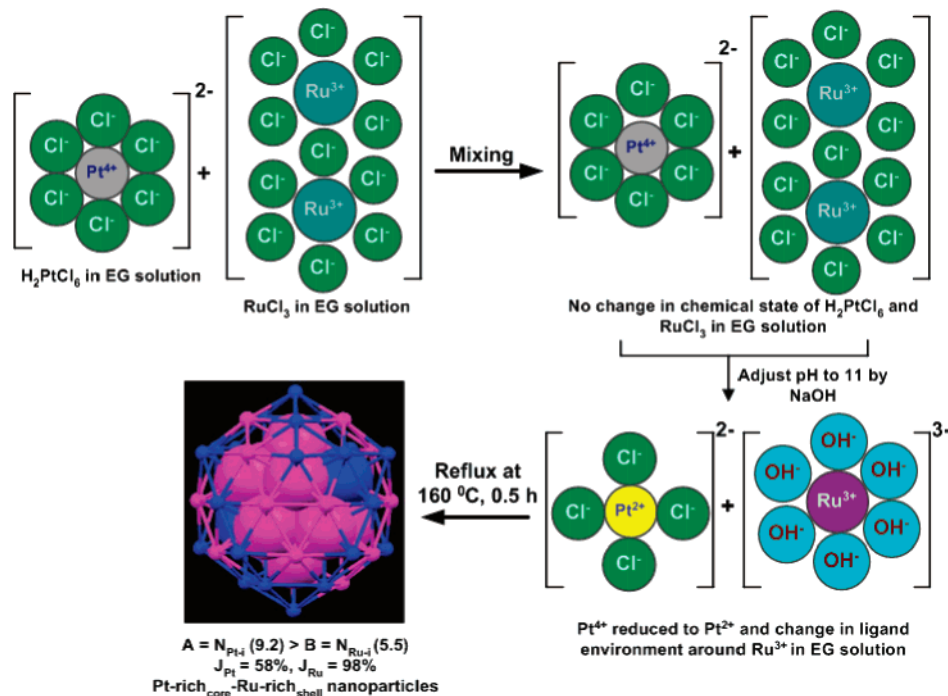
(18) Wyckoff, R. W. G. *Crystal Structure*, 2nd ed.; Interscience Publishers: New York, 1965; Vol. 3, p 69.

(19) (a) Yang, J.; Devivaraj, T. C.; Too, H.-P.; Lee, J. Y. *Langmuir* **2004**, *20*, 4241. (b) Wang, Z. L. *Adv. Mater.* **1998**, *10*, 13. (c) Fievet, F.; Lagier, J. P.; Blin, B.; Beaudoin, B.; Figlarz, M. *Solid State Ionics* **1989**, *32–33*, 198. (d) Tsuji, M.; Hashimoto, M.; Nishizawa, Y.; Kubokawa, M.; Tsuji, T. *Chem.–Eur. J* **2005**, *11*, 440.

Table 2. Best Fit Parameters Obtained from the Analysis of the Ru K Edge EXAFS Spectra of Various Reaction Steps during the Formation of Pt–Ru NPs^a

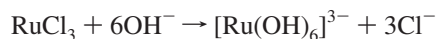
reaction state	shell	<i>N</i>	<i>R</i> (Å)	$\sigma^2 (\times 10^{-3})$ (Å ²)	ΔE_0 (eV)	<i>R</i> factor
RuCl ₃ in EG	Ru–Cl	6.0 (±0.1)	2.320 (±0.005)	9.0 (±0.5)	–6.5 (±0.9)	0.0280
RuCl ₃ + H ₂ PtCl ₆ in EG	Ru–Cl	6.0 (±0.1)	2.315 (±0.005)	8.7 (±0.5)	–5.8 (±0.5)	0.0200
pH control to 11	Ru–Cl	0.5 (±0.1)	2.408 (±0.001)	1.6 (±0.2)	13.4 (±1.5)	
	Ru–OH	4.9 (±0.1)	2.052 (±0.002)	4.2 (±0.2)	–0.5 (±0.4)	0.0026
reflux at 160 °C, 0.5 h	Ru–Pt	2.7 (±0.2)	2.745 (±0.005)	9.1 (±0.5)	1.3 (±0.5)	
	Ru–Ru	2.8 (±0.2)	2.735 (±0.004)	6.4 (±0.3)	12.4 (±1.3)	0.0350
reflux at 160 °C, 1 h	Ru–Pt	2.7 (±0.1)	2.743 (±0.004)	8.4 (±0.4)	0.6 (±0.2)	
	Ru–Ru	2.8 (±0.2)	2.735 (±0.005)	6.8 (±0.4)	11.9 (±1.1)	0.037
reflux at 160 °C, 2 h	Ru–Pt	2.7 (±0.3)	2.741 (±0.004)	7.8 (±0.4)	–0.4 (±0.3)	
	Ru–Ru	2.8 (±0.2)	2.735 (±0.005)	6.7 (±0.4)	11.6 (±1.1)	0.0420
reflux at 160 °C, 4 h	Ru–Pt	2.7 (±0.2)	2.745 (±0.004)	7.9 (±0.5)	1.1 (±0.2)	
	Ru–Ru	2.8 (±0.2)	2.735 (±0.004)	6.9 (±0.4)	12.3 (±1.2)	0.0340

^a *N* = coordination number, *R* = coordination distance, σ^2 = Debye–Waller factor, and ΔE_0 = inner potential correction.

Scheme 1. Schematic Presentation of All the Reaction Steps during the Formation of Pt–Ru Bimetallic NPs in EG Solutions^a

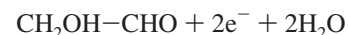
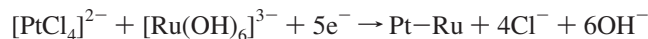
^a Key: pink, Pt; blue, Ru.

electrons were provided by the oxidation of ethylene glycol to glycolic acid. The present XAS results provide information about the stepwise reduction of metal ions, and we believe that the formation of $[PtCl_4]^{2-}$ and $[Ru(OH)_6]^{3-}$ upon adjustment of the pH of a solution containing H₂PtCl₆ and RuCl₃ in EG solution to 11 is associated with the following chemical reactions:



When the above reaction mixture containing the metal ion species $[PtCl_4]^{2-}$ and $[Ru(OH)_6]^{3-}$ is heated at 160 °C for about 0.5 h,

formation of Pt–Ru NPs is observed, and the corresponding chemical reactions can be written as



The coordination number derived from XAS is a strong and nonlinear function of the particle diameter up to 3–5 nm. This property has been widely used in EXAFS analysis to determine the size of the nanoparticle.² In the present study at the final step of the formation of Pt–Ru NPs the numbers of nearest neighbors around Pt and Ru are 9.2 and 5.5, respectively, giving an averaged first-shell coordination number of 7.3. This value corresponds to an average particle size of about 1.5–2 nm on the assumption

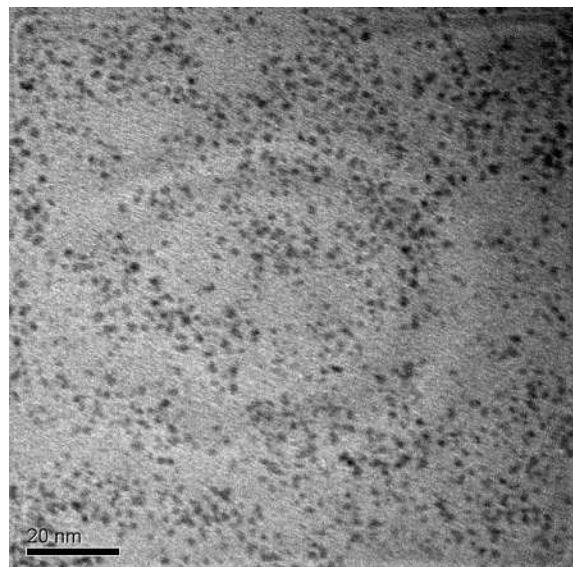


Figure 7. High-resolution TEM image of Pt–Ru particles in ethylene glycol solutions.

of a close-packed structure.²⁰ Figure 7 shows the typical high-resolution TEM image of Pt–Ru NPs of the final step. It can be seen that the particle distribution of the resultant Pt–Ru NPs is extremely uniform on the microscope grid. The mean diameter is estimated to be 1.5 nm from the TEM measurements. The particle size obtained from XAS is in good agreement with the TEM measurements.

The atomic distribution (or the alloying extent) of Pt and Ru in bimetallic nanoparticles plays a key role in determining their activity toward methanol oxidation. Earlier we proposed an XAS-based methodology to determine the atomic distribution (or alloying extent) in bimetallic nanoparticles.⁴ We have applied this methodology to Pt–Ru investigated here. In the case of Pt–Ru bimetallic clusters formed after the reaction mixture was refluxed at 160 °C for 0.5 h, the coordination numbers of Pt and Ru atoms around the Pt atom are found to be 6.5 and 2.7, respectively, and the total coordination number $\sum N_{\text{Pt}-i}$ ($= N_{\text{Pt}-\text{Pt}} + N_{\text{Pt}-\text{Ru}}$) is 9.2. The coordination numbers of Ru and Pt atoms around the Ru atom are determined to be 2.8 and 2.7, respectively, and the total coordination number $\sum N_{\text{Ru}-i}$ ($= N_{\text{Ru}-\text{Ru}} + N_{\text{Ru}-\text{Pt}}$) is calculated as 5.5. No change in either $\sum N_{\text{Pt}-i}$ or $\sum N_{\text{Ru}-i}$ is observed when the reflux time is increased. Hence, the alloying extent parameters calculated for Pt–Ru NPs are the same for all the time periods. From $N_{\text{Pt}-\text{Ru}}$, $\sum N_{\text{Pt}-i}$, $N_{\text{Ru}-\text{Pt}}$, and $\sum N_{\text{Ru}-i}$, structural parameters P_{obsd} ($N_{\text{Pt}-\text{Ru}}/\sum N_{\text{Pt}-i}$) and R_{obsd} ($N_{\text{Ru}-\text{Pt}}/\sum N_{\text{Ru}-i}$) are calculated as 0.29 and 0.49, respectively. Then the alloying extents of Pt (J_{Pt}) and Ru (J_{Ru}) are calculated by using eqs 1 and 2,

$$J_{\text{Pt}} = (P_{\text{obsd}}/P_{\text{random}}) \times 100 \quad (1)$$

$$J_{\text{Ru}} = (R_{\text{obsd}}/R_{\text{random}}) \times 100 \quad (2)$$

respectively, where P_{random} and R_{random} can be taken as 0.5 for perfect alloyed bimetallic NPs if the atomic ratio of Pt and Ru is 1:1. This value can be achieved by following the constraints of $N_{\text{Pt}-\text{Pt}} = N_{\text{Pt}-\text{Ru}}$ and $N_{\text{Ru}-\text{Ru}} = N_{\text{Ru}-\text{Pt}}$. By using eqs 1 and 2, the alloying extents of Pt (J_{Pt}) and Ru (J_{Ru}) are calculated as 58%

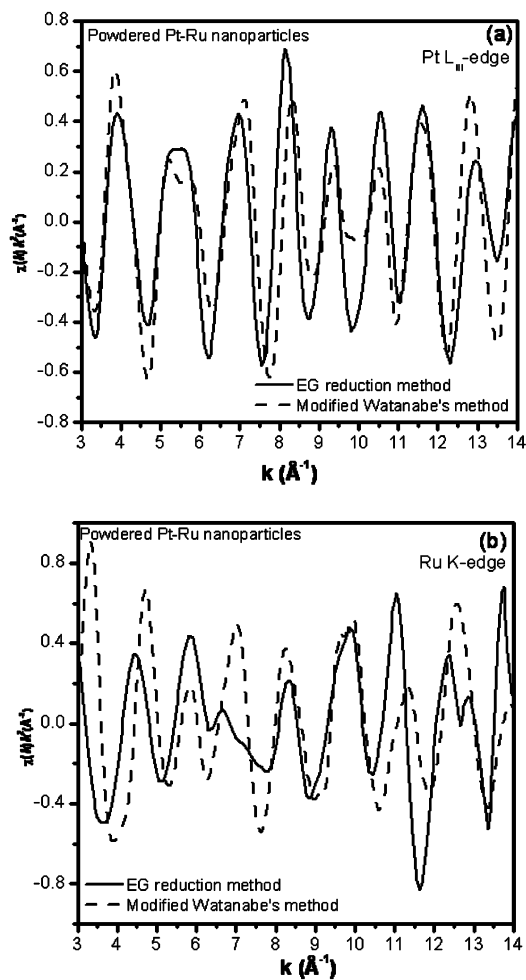


Figure 8. Raw $k^2\chi(k)$ (\AA^{-2}) EXAFS data of powdered Pt–Ru NPs collected at the (a) Pt L_{III} edge and (b) Ru K edge.

and 98%, respectively. The higher values of R_{obsd} , 0.49, and J_{Ru} , 98%, indicate the higher extent of atomic dispersion or the higher alloying extent of Ru atoms compared to Pt. The observed parameter relationships $\sum N_{\text{Pt}-i} > \sum N_{\text{Ru}-i}$ and $J_{\text{Ru}} > J_{\text{Pt}}$ indicate that the obtained Pt–Ru NPs adopt a Pt-rich core and Ru-rich shell structure. The observed parameter relationship, i.e., $\sum N_{\text{Pt}-i} > \sum N_{\text{Ru}-i}$, for the Pt–Ru nanoparticles investigated here is consistent with the relationship $N_{\text{AA}} + N_{\text{AB}} > N_{\text{BA}} + N_{\text{BB}}$ for a homogeneous system of A–B bimetallic NPs for which the core of the cluster is composed of N atoms of A (N_{A}) and the surface is made of N atoms of B (N_{B}), and the total coordination number ($N_{\text{AA}} + N_{\text{AB}}$) for the A atoms is greater than the total coordination for the B atoms ($N_{\text{BA}} + N_{\text{BB}}$).^{21,22} From the quantitative extent of alloying, we can see that, in Pt–Ru NPs synthesized by the EG reduction method, a considerable amount of Ru dominates in the shell region with a lower extent of segregation. The larger J_{Ru} value indicated that most of the Ru is involved in alloying and hence there is less segregation of Ru in the shell region (see the final product in Scheme 1). The lower $N_{\text{Ru}-\text{Ru}}$, 2.8, compared to $N_{\text{Pt}-\text{Pt}}$, 6.5, further supports less segregation of Ru in the shell region. The lower J_{Pt} value reveals that in the core homometallic Pt–Pt bonds are preferred rather than heterometallic Pt–Ru bonds. We compare the tight-binding Ising model (TBIM) prediction on the Pt–Ru system²³ with that

(21) Bazin, D.; Sayers, D.; Rehr, J. J. *J. Phys. Chem. B* **1997**, *101*, 11040.

(22) Via, G. H.; Sinfelt, J. H. In *X-ray Absorption Fine Structure for Catalysts and Surfaces*; Iwasawa, Y., Ed.; World Scientific: London, 1996.

(23) Bazin, D.; Mottet, C.; Trèglia, G. *Appl. Catal., A* **2000**, *200*, 47.

(20) (a) Gates, B. C.; Katzer, J. R.; Schuit, G. C. *Chemistry of Catalytic Processes*; McGraw-Hill: New York, 1979. (b) Greegor, R. B.; Lytle, F. W. *J. Catal.* **1980**, *63*, 476.

Table 3. Pt L_{III} Edge and Ru K Edge EXAFS Structure Parameters of Powdered Pt–Ru NPs Synthesized by the EG Reduction Method and Modified Watanabe Method^a

synthesis method	shell	<i>N</i>	<i>R</i> (Å)	$\sigma^2 (\times 10^{-3})$ (Å ²)	ΔE_0 (eV)	<i>R</i> factor
EG reduction	Pt–Ru	2.0 (±0.3)	2.716 (±0.005)	11.1	0.0	0.0249
	Pt–Pt	7.1 (±0.3)	2.764 (±0.005)	6.7	−5.8	
	Ru–Ru	3.1 (±0.2)	2.654 (±0.007)	5.0	−7.6	
	Ru–Pt	3.0 (±0.4)	2.716 (±0.006)	6.6	−5.2	
modified Watanabe	Pt–Ru	1.8 (±0.4)	2.700 (±0.003)	4.1	0.0	0.0168
	Pt–Pt	6.9 (±0.3)	2.747 (±0.005)	5.9	5.9	
	Ru–Ru	4.9 (±0.2)	2.669 (±0.008)	6.6	4.9	
	Ru–Pt	1.8 (±0.2)	2.700 (±0.004)	2.0	2.4	

^a *N* = coordination number, *R* = coordination distance, σ^2 = Debye–Waller factor, and ΔE_0 = inner potential correction.

of Pt–Ru nanoparticles in ethylene glycol solutions investigated here. For the Pt–Ru system IBIM predicts a tendency for phase separation (if the first-neighbor interaction in bimetallic nanoparticles, *V*, is <0). At sufficiently higher temperature near the thermodynamical equilibrium, Pt is found enriched at the surface, whereas low temperatures favor Ru enrichment. Our results show that, in Pt–Ru nanoparticles synthesized in ethylene glycol solutions at 160 °C, Pt dominates in the core region and Ru dominates in the shell region. Even though it appears that our experimental results are consistent with the theoretical predictions, a strict comparison cannot be made because the distribution of the two species inside the cluster is affected by the preparation conditions and relative reducibility of Pt and Ru ions in EG solutions.

We attempted to compare the alloying extents of Pt and Ru and their atomic distributions in the Pt–Ru NPs synthesized by the EG reduction method with those of the Pt–Ru NPs synthesized by the modified Watanabe method.³ To have a better comparison, the product obtained in the final step, i.e., reflux at 160 °C for 4 h, in the case of the EG reduction method, and the final product obtained from the modified Watanabe process were used. XAS measurements were performed on these two powdered samples. The raw *k*²-weighted Pt L_{III} edge and Ru K edge EXAFS data (Pt L_{III} edge, $\Delta k = 3.60\text{--}13.06 \text{ \AA}^{-1}$; Ru K edge, $4.17\text{--}12.19 \text{ \AA}^{-1}$) collected from the powdered samples of the Pt–Ru NPs synthesized by the EG reduction method and by the modified Watanabe method are presented in panels a and b, respectively, of Figure 8. EXAFS structural parameters obtained for the powdered Pt–Ru NPs synthesized by the EG reduction method and by the modified Watanabe method are listed in Table 3. The nearness in statistics of EXAFS parameters allowed us to compare the alloying extents of Pt (*J*_{Pt}) and Ru (*J*_{Ru}) of Pt–Ru NPs synthesized by the above-mentioned two methods.

The $P_{\text{obsd}} (=N_{\text{Pt–Ru}}/\sum N_{\text{Pt–i}})$ and $R_{\text{obsd}} (=N_{\text{Ru–Pt}}/\sum N_{\text{Ru–i}})$ are calculated as 0.22 and 0.49, respectively, for the powdered Pt–Ru NPs synthesized by the EG reduction method. In the case of the powdered Pt–Ru NPs synthesized by the modified Watanabe method, the P_{obsd} and R_{obsd} values are found to be 0.21 and 0.27, respectively. The higher P_{obsd} and R_{obsd} values in the case of the Pt–Ru NPs synthesized by the EG reduction method compared

to those synthesized by the modified Watanabe process suggest that the Pt and Ru atomic distribution in the former is much better than that in the latter. Similarly, the alloying extents of Pt and Ru were found to be higher in the case of the Pt–Ru NPs synthesized by the EG reduction method (*J*_{Pt} = 58%, *J*_{Ru} = 98%) compared to the Pt–Ru NPs synthesized by the modified Watanabe method (*J*_{Pt} = 42%, *J*_{Ru} = 54%). It appears that glycolate ion formed as a result of oxidation of ethylene glycol will act as a stabilizer for Pt–Ru particles and growth retardation of the nanoparticles may improve the corresponding distribution of Pt and Ru in Pt–Ru NPs. In this case the enhanced atomic distribution and uniformity in the resulting Pt–Ru NPs synthesized by the ethylene glycol reduction method make them attractive for methanol oxidation reaction.

Conclusions

In situ XAS experiments allowed us to characterize the successive steps of the Pt–Ru nanoparticle formation process during their preparation by the ethylene glycol reduction method. The XAS results demonstrate that well-defined Pt–Ru nanoparticles were formed at 160 °C reflux for 0.5 h of the reaction mixture. The stability of the Pt–Ru nanoparticles is extremely good as realized from no variation in XAS structural parameters at increased reflux time of the reaction mixture. The final Pt–Ru nanoparticles possess a structure similar to that of a Pt-rich core and a Ru-rich shell. On the basis of the XAS structural parameters, we found that the atomic-scale distribution of Pt and Ru is better in the final Pt–Ru NPs compared to the Pt–Ru NPs prepared by a modified Watanabe process. Extending this analysis to ion mixtures of different metals could give a simple but effective tool to evaluate multimetallic cluster formation mechanisms.

Acknowledgment. We gratefully acknowledge financial support from the National Science Council, use of facilities of the National Synchrotron Radiation Research Center (NSRRC), and financial support from the NRC-NSC-ITRI Initiative on Nanoscience and Nanotechnology and the National Taiwan University of Science and Technology, Taiwan, Republic of China.

LA0637418